Assessment of the Visible Channel Calibrations of the TRMM VIRS and MODIS on *Aqua* and *Terra*

Patrick Minnis

Science Directorate, NASA Langley Research Center,
Hampton, VA 23681 USA

David R. Doelling

Science Systems and Applications, Inc.
Hampton, VA 23666 USA

Louis Nguyen

Science Directorate, NASA Langley Research Center,
Hampton, VA 23681 USA

Walter F. Miller

Science Systems and Applications, Inc.
Hampton, VA 23666 USA

Venketesan Chakrapani
Hampton University
Hampton, VA 23666 USA

Submitted to *Journal of Atmospheric and Oceanic Technology*
April 2007

* Corresponding Author: , p.minnis@nasa.gov

ABSTRACT

Several recent research satellites carry self-calibrating multispectral imagers that can be used for calibrating operational imagers lacking complete self-calibrating capabilities. In particular, the visible (VIS, 0.65 μm) channels on operational meteorological satellites are generally calibrated before launch, but require vicarious calibration techniques to monitor the gains and offsets once they are in orbit. To ensure that the self-calibrating instruments are performing as expected, this paper examines the consistencies between the VIS channel (channel 1) reflectances of the Moderate Resolution Imaging Spectroradiometer (MODIS) instruments on the *Terra* and *Aqua* satellites and the Version 5a and 6 reflectances of the Visible Infrared Scanner (VIRS) on the Tropical Rainfall Measuring Mission using a variety of techniques. These include comparisons of *Terra* and *Aqua* VIS radiances with coincident broadband shortwave radiances from the well-calibrated Clouds and the Earth's Radiant Energy System (CERES), time series of deep convective cloud (DCC) albedos, and ray-matching intercalibrations between each of the three satellites. Time series of matched *Terra* and VIRS data, *Aqua* and VIRS data, and DCC reflected fluxes reveal that an older version (Version 5a, ending in early 2004) of the VIRS calibration produced a highly stable record, while the latest version (Version 6) appears to overestimate the sensor gain change by ~1% y^{-1} as the result of a manually induced gain adjustment. Comparisons with the CERES shortwave radiances unearthed a sudden change in the *Terra* MODIS calibration that caused a 1.17% decrease in the gain on 19 November 2003 that can be easily reversed. After correction for these manual adjustments, the trends in the VIRS and *Terra* channels are no greater than 0.1% y^{-1}. Although the results were more ambiguous, no statistically significant trends were found in the *Aqua* MODIS channel-1 gain. The *Aqua* radiances are 1% greater, on average, than their *Terra* counterparts, and after normalization are 4.6% greater than VIRS radiances, in agreement with theoretical calculations. The discrepancy between the two

MODIS instruments should be taken into account to ensure consistency between parameters derived from them. With the adjustments, any of the three instruments can serve as references for calibrating other satellites. Monitoring of the calibrations continues in near-real-time and the results are available via the world wide web.

1. Introduction

The NASA Earth Observing System (EOS) comprises an array of satellites and instruments designed to monitor many of the Earth's components and systems. Part of this array is used by the Clouds and Earth's Radiant Energy System (CERES; Wielicki et al., 1996; Smith et al., 2004) to improve our understanding of climate changes by determining the interaction between clouds and the Earth's radiation budget. This is being accomplished by simultaneously measuring broadband radiances and estimating cloud properties from imager measurements using data from three satellites, the Tropical Rainfall Measuring Mission (TRMM), *Terra*, and *Aqua*, to observe a given location at different times of day. One or two CERES broadband scanners are onboard each satellite. Additionally, the Visible Infrared Scanner (VIRS; Barnes et al., 2000) is on TRMM and the Moderate Resolution Imaging Spectroradiometer (MODIS; Barnes et al., 1998) is on both *Aqua* and *Terra*. The original vision to fuse together the 3-satellite dataset to cover the entire diurnal cycle was compromised by the failure of the CERES TRMM scanner in late 1998. Nevertheless, seven of the expected eight instruments are still operating at the time of this writing and the combined results will constitute a valuable climate data record if the parameters derived from each instrument are consistent in terms of processing and calibration. The former is a matter of applying identical methods to the various datasets while the latter requires self-monitoring and determination of the theoretical and empirical relationships between corresponding channels on each instrument. To ensure that this subset of the EOS array can be used to reliably monitor radiation and cloud parameters in a changing climate, it is critical that the relationships between the various instruments are characterized and used to remove any spurious anomalies.

The CERES scanner calibrations have been extensively studied and characterized in terms of absolute accuracy and trends (Priestley et al., 2000, 2003; Thomas et al., 2004; Wilson et al., 2003). Corrections have been developed to eliminate trends due to shortwave sensor degradation on the *Aqua* and *Terra* scanners (Spence et al., 2004; Matthews et al., 2005) resulting in a very stable climate record of broadband radiance and flux data. Monitoring and adjusting the calibrations of the 490 detectors used for the 36 MODIS narrowband channels on *Terra* and *Aqua* (e.g. Barnes et al., 2004) and the five VIRS channels is in itself a daunting task. To date, efforts to understand the relationships among the relevant channels on those three imagers have been fruitful, but extremely limited. Minnis et al. (2002a,b) and Lyu and Barnes (2003) each compared 1 month of matched radiances from the VIRS and corresponding *Terra* MODIS channels. Those same studies found conflicting trends in the VIRS visible (VIS, ~0.65 μm) channel calibrations. Using matched CERES shortwave (SW, 0.2 - 5 μm) and VIRS VIS radiances, Minnis et al. (2002a) found no statistically significant trends in the regression slopes between the CERES SW and VIRS reflectances over ocean between January and August 1998 and no differences between the single-month results for March 1998 and 2000. Lyu and Barnes (2003), however, found that the VIS channel response appeared to decrease by 1.15% y^{-1} based on roughly 20 lunar and deep-space calibration measurements each year between 1998 and the end of 2001. Subsequently, the VIS radiances are adjusted in the VIRS Version-6 datasets to minimize the impact of this apparent degradation in the sensor response (C.-H. Lyu, personal communication, 2005). Based on in-orbit measurements, Barnes et al. (2004) found that the *Terra* MODIS VIS (channel 1) response changed by less than 1% relative to its pre-launch values during its first 4.5 years of service. Similarly, the *Aqua* MODIS VIS response decreased by 3.1% during its first 2 years. However, the measured response changes are taken into account

in the calibrated radiances and, therefore, the data should exhibit no significant trends in calibration (X. Xiong, personal communication, 2005).

To further ensure consistency between the VIS channels on the various imagers, this paper directly compares the VIS radiances between each pair of instruments from the three satellites and the CERES SW and MODIS VIS radiances on *Terra* and *Aqua*. Both absolute differences and relative trends are examined to understand the relationships between the different imager VIS channels. The results of this analysis document the differences between the channels and will provide guidance for possible corrections to one dataset or another. Furthermore, since the MODIS and VIRS channels are used as references for calibrating other satellite imagers (e.g., Minnis et al., 2002a), this study will help minimize the introduction of any artificial trends in the corresponding channel radiances of those other instruments.

2. Data

All of the CERES, VIRS, and MODIS data were retrieved from NASA Langley Atmospheric Science Data Center. For reference, the VIS-channel spectral filter functions for each satellite are plotted in Fig. 1. The VIRS channel is considerably wider than either MODIS filter, which is nearly identical for *Aqua* and *Terra*. The former includes more Rayleigh scattering in the observed radiation field than the MODIS filter. Such differences must be taken into consideration when intercalibrating in absolute terms, but should have negligible effect on the relative trends studied here.

a. VIRS

TRMM was launched on November 27, 1997 and circles the Earth in a precessing 35°-inclined orbit where it observes areas equatorward of ~37° latitude at all local hours and viewing

zenith angles (VZA) up to 45°. The 2-km resolution VIRS calibrated radiances, based on pre-launch and on-board procedures (Barnes et al., 2000), were obtained the from level 1B01 Version-5a (V5) data through March 2004 and from Version 6 (V6) data thereafter. The V6 calibrations were also applied *post facto* to the radiances taken between 1998 and March 2004 to provide a complete up-to-date time series of V6 data. The VIRS calibration has been evaluated using comparisons with other self-calibrated satellite sensors (Minnis et al., 2002a) including the broadband CERES scanners (Wielicki et al., 1998), the second Along Track Scanning Radiometer (Smith et al., 1997), and the *Terra* MODIS, and using lunar models, solar calibrations, and MODIS data (Lyu and Barnes, 2003). Those comparisons provided calibration corrections for apparent trends in the data and demonstrated the stability of the instrument. The main difference in channel 1 between Versions 5a and 6, as noted earlier, is that the gain was corrected to account for an apparent linear degradation in the response determined from the solar measurements of Lyu and Barnes (2003) taken from 1998 through 2001. Based on the responsivities reported by Lyu and Barnes (2003), the gains for V5 and V6 are 0.01443 and $(0.01433 + DSR\ 0.483 \times 10^{-6})$ $Wm^{-2}sr^{-1}\mu m^{-1}C^{-1}$, where *DSR* is number of days since the reference date of 1 January 1998 and C is the observed brightness count.

The VIRS channel-1 (VIS) radiance is obtained from the following equation,

$$L_v = a(C - C_o) \qquad (1)$$

where a is the gain, and C_o is the space count. The VIRS solar constant E_v is 531.7 $Wm^{-2}sr^{-1}\mu m^{-1}$. For comparisons with MODIS data, the VIRS radiances are normalized as in Minnis et al. (2002a) to equivalent Geostationary Operational Environmental Satellite (GOES) radiances by

multiplying them by the ratio of the GOES and VIRS solar constants (E_o/E_v = 0.991). Here the nominal GOES solar constant E_o is 526.9 $Wm^{-2}sr^{-1}\mu m^{-1}$. To minimize the effects of parallax, navigation errors, and cloud advection, the VIRS radiances are averaged on a 0.5° equal angle grid for matching with *Terra* and *Aqua*.

b. MODIS

Terra MODIS began producing its first usable imagery during February 2000. It scans to a VZA of ~70° providing a swath that is 2330-km wide. *Aqua* MODIS started operational scanning in July 2002. *Terra* and *Aqua* have equatorial crossing times of 1030 LT and 1330 LT, respectively. Their orbital tracks nearly cross at 70°N and 70°S. A subset of the Collection-4, 1-km resolution *Terra* MOD021KM and *Aqua* MYD021KM data are used here (see http://daac.gsfc.nasa.gov/MODIS/products.shtml) through December 2005. Collection 5 data are used thereafter. The prelaunch calibration characteristics of the MODIS channels are discussed by Barnes et al. (1998). The MODIS radiances are computed in the same manner as the VIRS radiances where there is a gain and offset for each channel. For *Aqua*-*Terra*, the MODIS channel-1 (0.645 μm) radiances are averaged in circular regions with radii of 25 km. When compared with each other and CERES data, the *Terra* and *Aqua* MODIS VIS channels are assumed to be equivalent even though the solar constants, 509.3 and 510.0 Wm^{-2} μm^{-1} sr^{-1}, for their respective spectral filter functions differ by 0.12%. For comparison with the VIRS data, the *Terra* and *Aqua* radiances L_T and L_A, respectively, are normalized using the ratio of the GOES solar constant to 509.83 Wm^{-2} μm^{-1} sr^{-1}. This approach to inter-satellite calibration uses the GOES solar constant as a reference simply for convenience because it provides continuity with previous calibrations (Minnis et al., 2002a).

c. CERES broadband SW radiances

The CERES instruments on *Terra* and *Aqua* consist of two programmable scanners. One scanner operates primarily in the cross-track mode and the other mostly in the rotating-azimuth plane scanning (RAPS) mode. This study uses the unfiltered radiances taken between March 2000 and December 2005 and between July 2002 and March 2005 by the main cross-track scanners, flight models FM-1 and FM-4 on *Terra* and *Aqua*, respectively. The scanners have a nominal sub-satellite resolution of 20 km and view out to a nadir angle of 90°. Each radiance measurement is reported in the CERES Single Scanner Footprint (SSF) product (Geier et al., 2003), which includes many parameters including 1-km cloud products and selected raw MODIS radiances convolved into the CERES scanner field of view (Wielicki et al., 1998). Thus, the cross-track CERES radiances are optimally matched with the narrowband MODIS data in terms of space, time, and viewing angles. The instantaneous uncertainty in the unfiltered SW radiance is 0.6%. Each CERES radiance is classified as ocean, land, or desert based on the predominant surface type in the field of view.

This study uses CERES *Terra* Edition 2B and *Aqua* Edition 1B SSF cross-track data. Significant drifts in the FM-1 and FM-4 SW gains were found after processing of these editions began (Spence et al., 2004). Matthews et al. (2005) developed a set of scaling factors to account for the gain changes due to sensor degradation (http://eosweb.larc.nasa.gov/PRODOCS/ceres/SSF/Quality_Summaries/CER_SSF_Terra_Edition2B.html, http://eosweb.larc.nasa.gov/PRODOCS/ceres/SSF/Quality_Summaries/CER_SSF_Aqua_Edition2A.html). Those revisions (Rev1) are applied to all of the CERES radiances used here prior to comparison with the MODIS data. Initially, the resulting data were estimated to have a stability uncertainty of 0.12% y^{-1} (Matthews et al., 2005). More recent comparisons of 5.5 years of tropical CERES SW radiance

anomalies with their counterparts derived from extremely well-characterized VIS radiances from the Sea-Viewing Wide Field-of-View Sensor (Barnes et al., 2004; Eplee et al., 2005) indicate that the CERES *Terra* SW stability is on the order of 0.2 $\pm$ 0.5% per decade (Loeb et al., 2006). Comparisons of CERES *Aqua* and *Terra* anomalies between July 2002 and 2005 (Loeb et al., 2006) reveal that the Rev1-corrected *Aqua* SW radiances still retain a small trend of approximately -0.4% y^{-1} relative to those measured by *Terra* FM-1.

3. Methodologies

Two approaches are used here to assess the calibrations of the three imager VIS channels, cross-satellite and instrument correlations and deep convective cloud albedos. In these cross-satellite correlations, the calibration of the target satellite is adjusted to give new values that are consistent with the reference satellite.

a. Cross-satellite and instrument correlations

Minnis et al. (2002a) found that CERES and VIRS data taken over the ocean at solar zenith angles $SZA < 45°$ were optimal for examining relative trends between the respective broadband and narrowband channels. Therefore, only SSF data taken over water surfaces for $SZA < 45°$ and unaffected by sunglint are used here to determine a linear regression each day between MODIS and CERES on each satellite. Areas with significant sunglint were identified using the ocean bidirectional reflectance model of Minnis and Harrison (1984), which provides anisotropic correction factors χ as a function of viewing and illumination angles. For all values of *SZA*, pixels with $\chi > 1.4$ and a relative azimuth angle $RAA < 75°$ were assumed to be affected by sunglint and rejected. Pixels with $SZA < 25°$ and $\chi > 1.5$ for all values of *RAA* were also rejected.

For *Terra*,

$$L_{SWT} = a_T L_T + b_T, \quad (2)$$

where L_{SWT} is the CERES SW radiance. Likewise, for *Aqua*,

$$L_{SWA} = a_A L_A + b_A. \quad (3)$$

The relative trends in the calibrations are examined using two parameters: daily values of the slopes for variable offsets and for an offset forced to zero (average ratio of SW to VIS reflectances) for ocean only when SZA < 45° and daily mean ratios of the bidirectional reflectances for bright scenes (SW albedo exceeding 0.2) over all surfaces when SZA < 78°. The later are denoted as bright scene bidirectional reflectances (BRR).

The imager data are matched in the same manner used by Minnis et al. (2002a) to determine regression fits between the normalized 0.5° mean radiances. The correlations use those pairs of collocated radiances that are taken within 15 min of each other, are unaffected by sunglint, and have differences of less than 15° between their respective *VZA*s and *RAA*s. All of the correlations using VIRS data are based only on pixels taken over the ocean between 37°N and 37°S. The direct *Terra-Aqua* comparisons use data taken over oceans and the Antarctic and Greenland ice sheets as in Loeb (1997) and Tahnk and Coakley (2002) near 70° latitude. The data are matched every month for each pair of satellites.

The linear regression fits are formulated as follows. For the *Terra* and VIRS VIS channels,

$$L_T = a_{TV} L_V + b_{TV}, \quad (4)$$

where a_i and b_i are the regression-derived relative gains and offsets. The subscript letters refer to the particular pair of imagers. Similarly, for *Aqua* and VIRS,

$$L_A = a_{AV} L_V + b_{AV}. \quad (5)$$

Finally, the *Aqua* radiances are expressed in terms of the *Terra* values as

$$L_A = a_{AT} L_T + b_{AT}. \quad (6)$$

In addition to the standard regressions above, the least squares regression analyses were also performed while forcing the offset b_i to zero, and by switching the x-y axes and then computing the mean least-squares fit by averaging the x-y and y-x results. The former are referred to as force fits, while the latter are mean fits. Additionally, the slopes of the regression lines were also determined using principal component (PC) analysis. The temporal trends in the gains (slopes) and offsets are then computed using the values for all months together.

b. Deep convective cold cloud reflectance

Hu et al. (2004) pioneered the use of deep convective cloud (DCC) albedos as a means for estimating the relative stability of imager reflectance channels. Their approach assumes that, on average, the distribution of DCC broadband albedos remains constant over time. They used this approach along with narrowband-broadband conversion functions based on three reflectance

channels to examine the relative stability of the VIRS and *Terra* MODIS. Their results confirmed the conclusions of Minnis et al. (2002a) about the VIRS VIS stability between 1998 and 2000 and, based on 4 months of data, indicate that the *Terra* MODIS VIS channel is stable to within 1% between 2000 and 2002.

Doelling et al. (2004) used a similar approach with the same assumptions, but eliminated the conversion of the multispectral data to broadband albedos and developed a DCC Technique (DCCT) for estimating calibration trends directly for single-channel spectral data. The DCCT develops a probability distribution functions (PDF) of normalized VIS radiances each month over ocean for all pixels *i* between 30°N and 30°S that meet all of the following criteria:

$$T_{11i} < 205.0 \text{ K}, SZA < 40°, VZA < 40°, 10° < RAA < 170°, \sigma(T_{11}) < 1.0 \text{ K}, \text{ and } \sigma(\rho) < 0.02\ \rho_i,$$

where T_{11} is the 10.8-μm channel brightness temperature, σ is the standard deviation of the specified quantity for the subject pixel and its eight adjacent pixels, and ρ is the VIS reflectance. The value of L_i is first corrected for anisotropy to obtain a Lambertian-equivalent radiance L_{Ni} by multiplying by the appropriate theoretical DCC anisotropic correction factor from Hu et al. (2004). The resulting spectral radiance is then normalized to $SZA = 0°$ using the CERES SZA-dependent albedo model for overcast ice clouds over ocean with optical depths greater than 50 (Loeb et al., 2003). To ensure that the broadband CERES albedo model is applicable to the VIS data, all VIRS DCC L_N's for 1 month were averaged according to SZA and compared with the CERES albedo model applied to estimate the radiance at all SZAs given the radiance at 0°. The resulting radiance curves in Fig. 2 show that the predicted radiances are all within about 1% of the observed averages out to $SZA = 75°$. The normalized radiances taken during the month are then used to form a PDF and compute the mean and mode radiances.

4. Results

a. Cross-satellite and instrument correlations

1) VIRS VS. MODIS

The scatter plots and regression fits for matched VIRS and *Terra* MODIS data are shown in Fig. 3 for July 2000 and June 2005. During July 2000 (Fig. 3a), the average value of a_{VT} is 1.030 compared to 0.941 during June 2005 (Fig. 3b), a drop of 7.6%. The corresponding offsets change from -1.5 $Wm^{-2}sr^{-1}\mu m^{-1}$ to -0.4 $Wm^{-2}sr^{-1}\mu m^{-1}$. Thus, the relative change between the two calibrations is primarily due to gain changes in one or both of the imagers. The PC fits (not shown) yield values of a_{VT} that fall by 8.1% from 1.036 to 0.941, while the force fits produce a 7.4% decrease. The least squares regression was also applied to the data after switching the axes; the average gains computed from the original and reversed-axis data changed from 1.036 to 0.949, values similar to those from the PC analysis. In all cases, the slope changes are statistically significant at the 95% confidence level according to the student-t test.

The gains were computed for all of the matched data and are plotted in Fig. 4 for the standard regression fits using *Terra* and *Aqua* data. Of all of the various fits, the dataset with the least noise over time is that based on the standard least squares regression. The gains for each month are separated according to the VIRS version numbers and fit to a trend line of the form,

$$a_i = C_0 + C_1 \, DSR, \tag{7}$$

where the subscript i refers to a given satellite pair, time DSR is in the number of days since the reference date (usually since launch of reference satellite), and the gain at the reference data C_0 and the trend C_1 are found by least squares regression using the gains from the standard x-y fits

unless otherwise indicated. The trends in the VIRS V5a and V6 fits against *Terra* MODIS data (Fig. 4a) are dramatically different with the latter yielding average values around 0.945 compared to about 1.028 for the former. The trend lines indicate virtually no change (decrease of less than 0.1% y^{-1}) in the V5a slope, while the V6-*Terra* gains decrease at 1.4% y^{-1}. Time series of the slopes resulting from linear regression fits using matched VIRS and *Aqua* MODIS data are plotted in Fig. 4b along with the computed trend lines. Here, the mean slopes for VIRS V5 and V6 are 1.047 and 0.965, respectively. The *Aqua* slopes are almost 0.02 larger than their *Terra* counterparts. The trend line for V5-*Aqua* is slightly positive (0.1% y^{-1}) but not statistically significant. Conversely, the V6 trend line is negative with a 0.8% y^{-1} drop in the slope. Table 1 lists the trend line fits for both VIRS versions along with their corresponding squared linear correlation coefficients *R*.

2) *TERRA* VS. *AQUA* MODIS

Figure 5 plots the matched *Terra* and *Aqua* MODIS radiances and linear regression fits for July 2002 and 2005. The squared linear correlation coefficients are 0.99 for both plots with a slight increase in the slope between 2002 and 2005. This increase is confirmed in Fig. 6, which shows the average least squares fits and the gains for the fits forced to zero offsets. The relative gains from the PC fits (not shown) are identical to the mean least squares fits. The difference in the a_{AT} increase between the forced and mean fits is insignificant. Based on the mean fit results, *Aqua* radiances are 1% greater than their *Terra* counterparts at the beginning of the *Aqua* period and rise to 2.4% 3.25 years later. Overall, the *Aqua* radiances increase by 0.46 $\%y^{-1}$ relative to *Terra* each year.

The trend line from Fig. 6 for a_{AT} is

$$a_{AT} = 0.9253 \times 10^{-5}\, DSR + 1.0097, \quad (8)$$

where *DSR* is the *Aqua* launch date, 14 May 2002 . This result (see Table 1 also) suggests that the *Terra* MODIS channel-1 response has been degrading at roughly 0.34% per year relative to its *Aqua* counterpart.

3) CERES VS. MODIS

Scatterplots and the linear regression lines between the *Terra* and *Aqua* MODIS VIS and CERES FM-1 and FM-4 reflectances are shown in Fig. 7 for 15 March 2005. The *y*-intercepts blue line) and scatter for both are nearly equal while CERES observes a greater radiance for a given *Terra* VIS radiance than for a corresponding radiance from *Aqua* at larger values. Both force fits through the origin (red line) shift the same amount as the blue lines from *Terra* to *Aqua*. Thus, both the *Terra* regression slope and the average reflectance ratios are greater than those from *Aqua* for this day. Figure 8 shows time series of the gains from the daily linear regressions forced through the origin. The trend lines are also shown for each satellite. The trends from the variable intercept fits are similar. Only the slopes for the origin force fits are used hereafter to simplify the analysis by eliminating the offset. Both satellites show a seasonal cycle in the slope of the daily regression fits as the portions of the globe and the types of clouds sampled vary with the annual course of the sun. The regression slopes for *Terra* (Fig. 8a) appear to increase with time while those for *Aqua* (Fig. 8b) decrease slightly during the nearly 3 years of record. The trend line coefficients for the *Terra* and *Aqua* slopes are listed in Table 1 for the force fits through zero. The reference date, 1 January 2000, is the same for both lines.

To ensure that these trends are not limited to ocean surfaces and SZA < 78°, the mean bright scene BRRs were computed for each day. Seasonal variations in the BRR are evident (Fig. 9) but differ slightly from their counterparts in Fig. 8. However, the regression results (line not shown in Fig. 9), listed at the top of Table 2, are similar to the slope trends in that the *Terra* and *Aqua* reflectance ratios increase and decrease, respectively, with time. Since seasonal cycles are apparent in the data, trend lines were also computed using complete annual sets to determine if the trends seen in Fig. 8 and in the BRR trends are due to using data with incomplete annual cycles. Three trend lines were computed for each satellite as shown in Fig. 9. One uses all of the complete annual cycles starting at the beginning of the period, while the second bases the annual cycles from the end of the period. The third fit uses a complete set of years when the CERES scanner operated only in the cross-track scanning mode. The gaps seen in the early parts of the records in both Figs. 9a and 9b are primarily due to the scanner operating in the RAPS mode. Only cross-track data are considered here.

The BRR linear trend slopes and offsets for each set of conditions are listed in Table 2 with their corresponding squared linear correlation coefficients R. These can be compared to the coefficients for the entire period. The linear BRR fits are plotted over the daily values in Fig. 9. The *Terra* BRR trend lines using the first and last 5 years of data differ in slope by a little more than 50% but are visually difficult to distinguish from each other. During the first and last 5 years, the *Terra* BRRs increase by 0.27% and 0.39% y^{-1}, respectively. The trend during the 4 continuous years of cross-track FM-1 data is between the two 5-year trends. On the other hand, the *Aqua* ratios decrease by 1.31 and 0.41% y^{-1} for the first and last 3 years, respectively. The single year of continuous cross-track data yields a statistically insignificant rise in the BRRs of 1.24% y^{-1}. Additional data would be needed to obtain statistically meaningful results.

b. Deep convective cloud radiances

Figure 10 shows the monthly PDFs of VIRS Version 5a DCC pixel radiances observed between the DSR of 1 January 1998 and April 2003. While the width of the distributions varies, the mode values are all very consistent between 470 and 490 $Wm^{-2}sr^{-1}\mu m^{-1}$. All frequencies approach zero around 520 $Wm^{-2}sr^{-1}\mu m^{-1}$. The average mean and mode for the V5a period of record are 460 and 482 $Wm^{-2}sr^{-1}\mu m^{-1}$, respectively. For the V6 record, the corresponding values are 440 and 470 $Wm^{-2}sr^{-1}\mu m^{-1}$. The means and modes for each month were normalized by dividing each value by the period averages. The resulting trends for the normalized means are plotted in Fig. 11 along with the linear fits for each version. Time series from the normalized modes are very similar to those in Fig. 11 as indicated in the values listed in Table 3. The trend for the V5a normalized mean data (open circles) is $1.001 - 6.156 \times 10^{-7}$ d^{-1}, which translates to a statistically insignificant decrease of 0.02% per annum. The trend in the mode data translates to only -0.03% y^{-1}. Version 6 (solid squares) produces a very significant trend, $0.948 + 2.907 \times 10^{-5}$ d^{-1}, in the normalized DCC radiances that converts to an 8.9% rise over 9 years. This result is similar to that found in Fig. 4a.

The *Terra* and *Aqua* MODIS DCC normalized mean and mode radiance trends were computed in a similar manner and are plotted in Fig. 12 and listed with their VIRS counterparts in Table 2. The trends for the mean and mode for *Terra* (Fig. 12a) are nearly identical with an average value of -7.77×10^{-6} d^{-1}, which translates to a decrease of 2.8% per decade. The *Aqua* mean trend (Fig. 12b) is similar in magnitude, but positive, while the mode trend is slightly negative. The *Aqua* mean trend, 1.36×10^{-5} d^{-1}, is significantly different from zero at the 90% confidence level. The average trend for the two components is 6.0×10^{-6} d^{-1}, or 2% y^{-1}. Because

of the discrepancy between the mode and mean trends, it is difficult to conclude that the *Aqua* trend is significant overall.

5. Discussion

The results indicate some trends in the VIS channels of VIRS V6 and *Terra* MODIS, as well as an apparent trend in either the MODIS VIS or CERES SW channels on *Aqua*.

a. Apparent trend in Terra VIS channel

Comparisons between the *Terra* CERES SW and the MODIS VIS channels (Figs. 8a and 9a) and between the *Aqua* and *Terra* VIS channels (Fig. 6) together with the DCC analyses (Fig. 12) suggest that the response of the *Terra* VIS channel is degrading and the gain has not been increased sufficiently over the course of its lifetime through the onboard calibration process. The trends in the gain range from -0.23 to -0.34% y^{-1} for the CERES and *Aqua* comparisons, respectively. The magnitude of the former is similar to the DCC analysis, while the latter number is based on a shorter period and assumes stability in the *Aqua* response. Using daily averages of *Terra* CERES SW and MODIS VIS channel, near-nadir tropical radiances, Loeb et al. (2006) found that the relative stability of the CERES/MODIS data relative to 2000 was better than 1% y^{-1}. Their Fig. 2 shows that between 2000 and 2001, the mean CERES radiance decreased relative to the MODIS radiance by 0.5% and remained between 0.5 and 0.8% through 2003. It then increased abruptly up to values between 0.05 and 0.2% greater than the year 2000 values.

Those results are somewhat at odds with the findings in Figs. 8a and 9a. The latter suggests that if anything, the CERES SW slightly increased relative to MODIS during 2001 - 2003 relative to 2000. A close examination of Fig. 8a reveals a semi-annual cycle with peaks

around the equinoxes (days 80 and 267) and minima around the solstices (days 171 and 354). The cycles are ill-defined during the first 2 years because the FM-1 scanner was intermittently placed in the RAPS mode resulting in some significant data gaps. Although no cross-track data are available for day 80 during 2001 (day 445), the maximum slopes during 2000 are nearly identical to those seen during the period from 2001 through 2003, but the peak slopes during 2004-2005 are 1.5% greater than those during the previous 4 years. That relative difference is somewhat consistent with the results of Loeb et al. (2006) and is similar to the variations in Fig. 9a. The discrepancy between the present results and those from Loeb et al. (2006) for the 2001-2003 period relative to the 2000 baseline reference is likely due to a combination of effects. The Loeb et al. (2006) spatial and angular sampling is different and the large gaps during 2000 probably biased the mean radiances and slopes for that year compared to the other years, especially 2002 and 2003. Based on the maximum slopes during each year, it appears that differences between the first and the following 3 years are negligible, but are significant during the final 2 years.

Further examination of the time series in Fig. 8a reveals a sudden shift of 1% or more in the slope around day 1415 (15 November 2003). Review of the channel-1 calibration gains revealed that the LUTs for the reflective channels were updated every 2 weeks or so. The *Terra* MODIS channel-1 gain increased by 0.06% and 0.23% on October 3 and 21, respectively. The next change, a decrease of 1.17% from 0.027041 to 0.026729, was implemented on November 19, day 1419, which corresponds to the jump in Fig. 8a. Typically, the gain changes prior to that time were on the order of 0.03%. Despite the relatively frequent LUT changes, there appear to be no other discontinuities in the CERES-MODIS time series (Fig. 8a) of the magnitude seen on 1419. Using data taken separately before and after day 1419, the trends for the earlier and later

periods are -8.950 x 10^{-7} μm d^{-1} and -3.405 x 10^{-6} μm d^{-1}, respectively, while the corresponding offsets are 0.7121 and 0.7242, a 1.6% difference. The trends translate to -0.05 and -0.17% y^{-1}, respectively, and are not statistically significant. Using those trends and offsets, the respective slopes on day 1419 are 0.7108 and 0.7194, a 1.21% difference, a value very close to the 1.17% decrease in the gain that occurred on day 1419. This result along with the comparison with CERES suggests that the LUT change on day 1419 was too large and that subsequent changes did not rectify the difference.

The reason for this relatively large change in the calibration is not clear. Consultation of the *Terra* MODIS LUT history (http://www.mcst.ssai.biz/L1B/L1B_docs/V4_LATEST_L1B_DOCUMENTS/L1B_Terra_LUT_History.txt) reveals that a different set of LUTs was generated for the period from July 2 through October 31, 2003 for a non-production dataset (*V4.3.0.2M_Terra*) to account for an under-correction that apparently resulted from using a degradation trend algorithm based on data prior to July 2 instead of using the actual solar diffuser measurements. The latter were not used because the solar diffuser door was left open on July 2. Since the CERES-MODIS slopes (Fig. 8a) taken after 1418 are clearly greater than their pre-1419 counterparts, it is unlikely that changing the data between July 2 and October 31 during 2003 would remove the discontinuity; they would only change its time of occurrence. At the time of this writing, it is not clear that the discontinuity was removed in the special dataset. It appears that the discontinuity has been replaced by linear interpolation in the *Terra* MODIS Collection 5 dataset, but that the plateau in the calibration after day 1418 remains.

Figure 13 explores what happens to the calibrations if the *Terra* MODIS radiances are increased by 1.17% after day 1418, a correction that accounts for the change found in the MODIS calibration record discussed above. The mean radiances from Fig. 12a before and after

day 1418 are indicated in solid squares and open triangles, respectively, in Fig. 13a. The open squares in Fig. 13a are the result of increasing the normalized radiances after day 1418 by 1.17%. Using all of the data corresponding to the squares in Fig. 13a yields a DCC slope for *Terra* of 2.151 x 10^{-6} d^{-1}, a value (0.079% y^{-1}) that is insignificantly different from zero. Thus, assuming a 1.17% offset in the LUTs on day 1419 eliminates the apparent trend in the *Terra* channel-1 gain. These results strengthen the findings of Loeb et al. (2006). By accounting for more of the sampling gaps here and applying the 1.17% adjustment after day 1418 to the linear fit slopes in Fig. 8a, the trend in the slopes is -0.06% y^{-1}. The range in the annual mean slopes is only 0.46% with an average interannual difference of less than 0.1% y^{-1}. This result between the *Terra* MODIS VIS and CERES SW channels is substantially better than the 1% y^{-1} interannual stability found by Loeb et al. (2006).

Applying that same correction, dividing the relative gains by 1.0117, to the relative gains in Fig. 6 after day 567 (corresponds to 1418 in Fig. 13) yields the points and regression fit shown in Fig. 13b. Two trends are shown. The standard linear regression slope (denoted as x-y) is only -0.08% y^{-1}, and the trend based on forcing each fit to go through the origin is -0.02% y^{-1}. Both trends are statistically insignificant and confirm, that with the correction for the *Terra* discontinuity, the *Terra* VIS channel is stable to better than less than 0.1% y^{-1}. Even with the correction, the radiances measured by *Aqua* are, on average, 1.0% greater than those from *Terra*. Thus, to ensure consistency between the two sensors, one of the two calibrations must be normalized to the other.

b. Aqua trends

The results so far indicate that the *Aqua* MODIS VIS channel gain has changed by a negligible amount (Fig. 12b mode plot and Fig. 13b) up to 0.27% y^{-1} (Fig. 12b mean plot). Comparison with the CERES SW in Fig. 8b suggests that the *Aqua* VIS gain increased by 0.31% y^{-1} or the CERES SW decreased by the same amount. The results in Fig. 9b for the last 2 years of the data record (the first 2 years contain too many missing data points for a reliable trend), produce a drop of -0.41% y^{-1}. As noted earlier, Loeb et al. (2006) found that the *Aqua* CERES SW fluxes decreased by -0.40%y^{-1} relative to their *Terra* counterparts. A similar result, -0.37% y^{-1} (G. Matthews, personal communication 2006), was found using a DCC analysis of the CERES SW data (Matthews et al., 2006). Given the consistency between the various results, it is concluded that the trends in Figs. 8b and 9b are almost entirely due to the degradation in the CERES SW instrument and that the mean trend in Fig. 12b does not represent the true degradation in the *Aqua* VIS channel response. The trends in Fig. 13b and the mode variation in Fig. 12b suggest that the *Aqua* VIS channel response, like that for *Terra*, degrades at less than 0.1% y^{-1}. Further uncertainties in the *Aqua* trend are examined in the next section.

c. Trend in VIRS VIS channel

From the comparisons in Fig. 4 and the results in Fig. 11, it is clear that the VIRS V6 calibration has a significant trend. Lyu and Barnes (2003) developed the responsivity (gain) correction for V6 based on observations of the sun through the VIRS solar diffuser. Because the radiance observed through the diffuser decreased almost linearly at a rate of 1.15% y^{-1} during the first 4 years of operation and no change was seen in the corresponding channel-2 (1.6 μm) radiances, it was assumed that the sensor response was degrading, not the diffuser reflectivity. The trend in the V6 normalized gain in Fig. 11 is 1.04% y^{-1}, a value that is 10% smaller in

magnitude than the operational correction applied to the gain in V6. If the sensor response were degrading as predicted, then the V5 DCC data should have produced a decrease in the normalized gain and the V6 DCC trend should have been negligible. For the same period (DSR = 0 - 1460) used by Lyu and Barnes (2003), the relative change in the average of the mean and mode V5a DCC radiances is -0.17%y^{-1}, a value suggesting much less degradation in the channel-1 sensor than expected. Preliminary DCC analyses of the V5a and V6 VIRS channel-2 mode gains yield trends of 0.14 and 0.08% y^{-1}, respectively, confirming that there is no degradation in channel-2 sensor. Lyu and Barnes (2003) had no other information to assess their conclusion that the channel-1 sensor, rather, than the solar diffuser, was degrading. The additional data examined here suggest that there is no degradation in the solar diffuser.

To determine how this V6 trend impacts the intercalibrations with *Terra*, the V6 points in Fig. 4a were multiplied by the DCC trend values, computed from the mean and mode fits in Table 3, to yield V6' values. These are replotted in Fig. 14a along with the original V5a points (solid squares). The resulting linear fit yields a slightly negative trend (Table 4). However, it was found earlier that the *Terra* gain decreased by 1.17% on day 1419. Thus, the slopes determined after that date were multiplied by 1.0117 to account for the *Terra* change. These points (open circles) are easily seen above their original values in Fig. 14a. A final correction is needed to account for the change in responsivity between V5a and V6. The initial V5a channel-1 responsivity, 69.30 counts / (mW cm^{-2} sr^{-1} μm^{-1}), reported by Lyu and Barnes (2003) is nominally 0.7% less than their V6 value of 69.782 counts / (mW cm^{-2} sr^{-1} μm^{-1}). To achieve consistency with the V6' gains, the V5a gains, a_{TV5a}, were divided by 0.993 to obtain the V5a' gains, $a_{TV5a'}$, which are plotted as open triangles in Fig. 14a. Note that three of the gains, determined between days 1440 and 1560, were adjusted with both correction factors. The

resulting linear fit to the combined V5a' and V6' gains is shown as the solid line in Fig. 14a. The trend line coefficients are listed in Table 4. After applying both correction factors, the apparent trend in the *Terra* MODIS gains relative to VIRS is -0.02% y^{-1}, a statistically insignificant value.

Similarly, the V6' values were computed for the VIRS-*Aqua* slopes and plotted as solid squares in Fig. 14b along with the V5 results from Fig. 4b. The resulting linear fit (dashed line) yields a slightly negative trend (Table 4) that becomes more negative (solid line) when the 0.7% responsivity correction is applied to the V5a data resulting in the V5a' values (open circles). Without the correction, the slopes decrease at a rate of 0.06% y^{-1}, an insignificant trend. With the correction, the *Aqua*-VIRS slopes drop at 0.30% y^{-1} (Table 4), however, this trend is not significant at the 90% confidence level. It suggests that *Aqua* response is degrading or that the VIRS sensor is becoming more sensitive over time. Given the other trend evidence for *Aqua* discussed in the previous section the insignificance of this trend, it concluded again that the *Aqua* visible channel has not suffered any significant degradation.

d. Summary

Only a few corrections are needed to achieve constancy better than 0.1-0.2% in the VIRS and *Terra* and *Aqua* MODIS visible channel calibrations. When using VIRS V5a data, the radiances should be corrected to the V6 responsivity by dividing by 0.993. The VIRS V6 data should be adjusted using a correction based on the DCC normalized radiance trends in Table 3, either the mode trend or an average of the mean and mode trends. The *Terra* radiances should be increased by dividing by 1.0117 after 18 November 2003 to account for the shift in the *Terra* gain. No correction to the *Aqua* data appears to be necessary.

The only remaining differences between the sensors are their absolute calibrations. At the middle of their respective VIRS-matched time intervals, the *Terra* and *Aqua* radiances are 1.0352 and 1.0464, respectively, greater than their normalized VIRS counterparts. Likewise, the *Aqua* radiances are 1% greater than those from *Terra*. To explore theoretically how the different sensors should be related, the spectral response functions in Santa Barbara DISORT Atmospheric Radiative Transfer program (Richiazzi et al., 1998) and computations were performed over an ocean surface at several solar zenith angles using various aerosol types and concentrations and several cloud cover conditions. According to the theoretical calculations, the *Aqua* radiances should be, on average, 0.05% less than those from *Terra*. Thus, the differences between the Terra and Aqua found here are due to calibration. It was also found that the MODIS radiances, after normalization should be, on average, 1.048 greater than their VIRS counterparts. That value is very close to the mean slope found from the final VIRS-*Aqua* trend in Table 4 and differs by only 1% from the VIRS-*Terra* slope.

While the consistency between the *Aqua* and VIRS data suggest that both have excellent absolute calibrations and that either instrument could be a reliable reference, the consistency could be fortuitous and both gains could be off by the same amount. Determining which instrument has the best absolute calibration is beyond the scope of this paper.

6. Concluding Remarks

The comparisons presented in this paper confirm that the EOS imager visible channels have been remarkably well calibrated. Despite the artificially induced calibration change, the VIRS calibration is extremely stable. Obtaining degradation rates of less than 0.1% y^{-1} in three different sensors with absolute differences between them of 1% or less is a noteworthy

accomplishment. Only a few adjustments are needed to reconcile all three sensors, so that they should yield very consistent surface and atmospheric physical parameters when the retrieval algorithms account for their spectral differences. Furthermore, after corrections, any of the three instruments could serve as references for calibrating other satellite imagers, especially those operational meteorological satellites that have no onboard calibration systems for their visible channels.

Use of several different approaches is essential for evaluating satellite sensor calibrations. The comparisons with the CERES SW data were crucial for identifying the sudden change in the *Terra* MODIS gain and provided redundancy for some of the ambiguous results from other methods. The DCC method provides an independent assessment of each instrument. When both the mode and mean trends agree, the result is clear, but the differences in the *Aqua* trends introduce some uncertainty, which requires other yardsticks, like the CERES and *Terra* comparisons, to resolve the ambiguity. In that case, it appears that the mode trend was the more reliable of the two. As long as a satellite instrument is operational, its calibration will be an issue. To help ensure that no sudden changes or other trends are not overlooked, the intercalibrations described here will continue as long as possible. Results of the near-real-time monitoring of the intercalibrations and the historical results from this study are available on the world wide web at http://www.nasa.gov/centers/langley/science/satellite_calibration.html.

Acknowledgments. The research was supported by the NASA Science Mission, Radiation Sciences Branch through the Clouds and the Earth's Radiant Energy System Project. All data used in this study were obtained from the Atmospheric Sciences Data Center at NASA Langley Research Center.

REFERENCES

Barnes, R. A., W. L. Barnes, C.-H. Lyu, and J. L. Gales, 2000: An overview of the Visible and Infrared Scanner radiometric calibration algorithm. *J. Atmos. Ocean. Tech.*, **17**, 395-405.

Barnes, R. A., R. E. Eplee, Jr., F. S. Patt, H. H. Kieffer, T. C. Stone, G. Meister, J. J. Butler, and C. R. McCain, 2004: Comparison of SeaWIFS measurements of the Moon with the U.S. Geological Survey lunar model. *Appl. Opt.*, **43**, 5838-5854.

Barnes, W. L., T. S. Pagano, and V. V. Salomonson, 1998: Prelaunch characteristics of the Moderate Resolution Imaging Spectroradiometer (MODIS) on EOS–AM1. *IEEE Trans. Geosci. Remote Sens.,* **36,** 1088–1100.

Barnes, W., X. Xiong, and V. Salomonson, 2004: MODIS instrument status and operational activities. *Proc. SPIE Conf. Earth Observing Systems IX*, Denver, CO, Aug. 2-6, **5542**, 14-23.

CERES Science Team, 2005: CERES ES8 Terra Edition 2 Data Quality Summary. (Available at http://eosweb.larc.nasa.gov/PRODOCS/ceres/ES8/Quality_Summaries/CER_ES8_Aqua_Edition2.html)

CERES Science Team, 2005: CERES ES8 Aqua Edition 2 Data Quality Summary. (Available at http://eosweb.larc.nasa.gov/PRODOCS/ceres/ES8/Quality_Summaries/CER_ES8_Terra_Edition2.html)

Doelling, D. R., L. Nguyen, and P. Minnis, 2004: On the use of deep convective clouds to calibrate AVHRR data. *Proc. SPIE 49th Ann. Mtg., Earth Observing Systems IX Conf.*, Denver, CO, August 2-6, **5542**, 281-289.

Eplee, R. E. , Jr., R. A. Barnes, F. S. Patt, G. Meister, and C. R. McClain, 2004: SeaWiFS lunar calibration methodology after six years on orbit. *Proc. SPIE Earth Observing Systems IX*, **5542**, doi:10.1117/12.556408.

Geier, E. B., R. N. Green, D. P. Kratz, P. Minnis, W. F. Miller, S. K. Nolan, and C. B. Franklin, 2003: Clouds and the Earth's Radiant Energy System Data Management System Single Satellite Footprint TOA/Surface Fluxes and Clouds (SSF) Collection Document, Release 2, Version 1. 243 pp. (http://asd-www.larc.nasa.gov/ceres/collect_guide/SSF_CG.pdf).

Hu, Y., B. A. Wielicki, P. Yang, P. W. Stackhouse, Jr., B. Lin, and D. F. Young, 2004: Application of deep convective cloud albedo observation to satellite-based study of the terrestrial atmosphere: monitoring the stability of spaceborne measurements and assessing absorption anomaly. *IEEE Trans. Geosci. Remote Sens.*, **42**, 2594-2599.

Loeb, N.G., 1997: In-flight calibration of NOAA AVHRR visible and near-IR bands over Greenland and Antarctica. *Int. J. Remote Sens.*, **18**, 477-490.

Loeb, N. G., N. Manalo-Smith, S. Kato, W. F. Miller, S. Gupta, P. Minnis, and B. A. Wielicki, 2003: Angular distribution models for top-of-atmosphere radiative flux estimation from the Clouds and the Earth's Radiant Energy System instrument on the Tropical Rainfall Measuring Mission satellite. Part I: Methodology. *J. Appl. Meteorol.*, **42**, 240-265.

Loeb, N. G., B. A. Wielicki, W. Su, K. Loukachine, W. Sun, T. Wong, K. J. Priestley, G. T. Matthews, W. F. Miller, and R. Davies, 2006: Multi-instrument comparison of top-of-atmosphere reflected solar radiation. Accepted, *J. Climate*.

Lyu, C.-H., and W. L. Barnes, 2003: Four years of TRMM/VIRS on-orbit calibrations and characterization using lunar models and data from Terra/MODI*S. J. Atmos. Ocean. Tech.*, **20**, 333-347.

Matthews, G., K. Priestley, N. G. Loeb, K. Loukachine, S. Thomas, D. Walikainen, B. A. Wielicki, 2006: Coloration determination of spectral darkening occurring on a broadband Earth observing radiometer: application to Clouds and the Earth's Radiant Energy System (CERES). *Proc. SPIE Earth Observing Systems XI*, **6296**, paper no. 6296-25.

Matthews, G., K. Priestley, P. Spence, D. Cooper, and D. Walikainen, 2005: Compensation for spectral darkening of short wave optics occurring on the Clouds and the Earth's Radiant Energy System. *Proc. SPIE Earth Observing Systems X*, **5882**, doi:10.1117/618972.

Minnis, P., L. Nguyen, D. R. Doelling, D. F. Young, W. F. Miller, and D. P. Kratz, 2002a: Rapid calibration of operational and research meteorological satellite imagers, Part I: Evaluation of research satellite visible channels as references. *J. Atmos. Oceanic Technol.*, **19**, 1233-1249.

Priestley, K. J., and co-authors, 2000: Postlaunch radiometric validation of the Clouds and the Earth's Radiant Energy System (CERES) Proto-Flight Model on the Tropical Rainfall Measuring Mission (TRMM) spacecraft through 1999. *J. Appl. Meteor.*, **39**, 2249-2258.

Priestley, K. J., S. Thomas, P. L. Spence, Z. P. Szewczyk, E. A. Kizer, D. Walikainen, A. Al-Hajjah, and R. S. Wilson, 2003: A comprehensive radiometric validation protocol for the CERES Earth Radiation Budget climate record sensors. *Proc. SPIE Earth Observing Systems VIII*, **5151**, 282-287.

Richiazzi, P., S. Yang, C. Gautier, and S.D. Sowle, 1998: SBDART: A research and teaching software tool for plane-parallel radiative transfer in the Earth's atmosphere. *Bull. Amer. Meteorol. Soc.*, **79**, 2101-2114.

Smith, D. L., P. D. Read, and C. T. Mutlow, 1997: The calibration of the visible/near infra-red channels of the Along-Track Scanning Radiometer-2 (ATSR-2). *Sensors, Systems and Next Generation Satellites,* H. Fujisadsa, Ed., Proceedings of SPIE, Vol. 3221, International

Society for Optical Engineering, 53–62.

Smith, G. L., and co-authors, 2004: Clouds and Earth Radiant Energy System: An overview. *Adv. Space Res.*, **33**, 1125-1131.

Spence, P., K. Priestley, E. Kizer, S. Thomas, D. Cooper, and D. Walikainen, 2004: Correction of drifts in the measurement of the Clouds and Earth's Radiant Energy System scanning thermistor bolometer instruments on the Terra and Aqua satellites. *Proc. SPIE Earth Observing Systems IX*, **5542**, 53-64.

Tahnk, W. R. and J. A. Coakley, Jr., 2002: Improved calibration coefficients for the NOAA-12 and NOAA-15 AVHRR visible and near-IR channels. *J. Atmos. Ocean. Tech.*, **21**, 1826-1833.

Thomas, S., K. J. Priestley, and P. Spence, 2004: Performance results of CERES instrument sensors aboard EOS Terra and Aqua spacecraft using tropical ocean measurements. *Proc. SPIE Earth Observing Systems IX*, **5542**, 65-73.

Wielicki, B. A., B. R. Barkstrom, E. F. Harrison, R. B. Lee III, G. L. Smith, and J. E. Cooper, 1996: Clouds and the Earth's Radiant Energy System (CERES): An Earth Observing System Experiment, Bull. Amer. Meteor. Soc., 77, 853-868.

Wielicki, B. A., and co-authors, 1998: Clouds and the Earth's Radiant Energy System (CERES): Algorithm Overview. *IEEE Trans. Geosci. and Rem. Sens.*, **36**, 1127-1141.

Wilson, R. S., R. B. Lee, III, J. Paden, D. K. Pandey, K. J. Priestley, S. Thomas, and A. Al-Hajjah, 2003: On-orbit solar calibrations using the Aqua Clouds and Earth's Radiant Energy System (CERES) in-flight calibration system. *Proc. SPIE Earth Observing Systems VIII*, **5151**, 288-299.

Figure Captions

Fig. 1. Channel-1 spectral response functions.

Fig. 2. Mean anisotropically adjusted radiances as a function of SZA for deep convective clouds observed from VIRS during 1998 and for the normalized CERES SZA-dependent model for ice clouds with optical depths > 50 as calibrated using the VIRS average radiance at SZA = 0°.

Fig. 3. Scatterplots and regression fits between VIRS and *Terra* MODIS VIS channels, (a) VIRS V5a, (b) VIRS V6.

Fig. 4. Time series and least squares trends in gains computed between VIRS Versions V5a and V6 and (a) *Terra* and (b) *Aqua* MODIS channel-1 radiances.

Fig. 5. Scatterplots and regression fits between *Terra* and *Aqua* MODIS VIS channels.

Fig. 6. Time series and least squares trends in gains computed for *Aqua* relative to *Terra* MODIS channel-1 radiances.

Fig. 7. Scatterplots and linear regression fits of matched CERES broadband SW and MODIS VIS radiances over ocean for 0° < SZA < 45°, 15 March 2005.

Fig. 8. Time series of daily regression slopes between CERES SW and MODIS VIS radiances over ocean for SZA between 0 and 45°. Force-fit through origin.

Fig. 9. Time series of daily mean bright scene bidirectional reflectance ratios of CERES SW to MODIS VIS radiances over all surfaces for SZA < 78°.

Fig. 10. Monthly histograms of DCC radiances from VIRS Version 5a for SZA < 75°, January 1998 – April 2003.

Fig. 11. Monthly mean DCC radiances normalized to the mean for the period of record for each VIRS version. Lines indicate linear regression fits.

Fig. 12. Monthly mean and mode DCC radiances normalized to average for period of record for each MODIS VIS channel. Solid and dashed lines indicate regression fits for mean and mode, respectively.

Fig. 13. (a) Monthly mean *Terra* MODIS VIS DCC radiances before (solid squares) and after (open triangles) day 1418 normalized to average for entire period of record. Open squares are normalized DCC radiances taken after day 1419 that were adjusted by 1.21%, the apparent offset found using the CERES SW - *Terra* VIS trend analyses. Line corresponds to linear regression using data corresponding to all squares. Compare to trend line in Fig. 12a. (b) Same as Fig. 6, except mean values only divided by 1.0121 after day 547. Compare to dashed line in Fig. 6.

Fig. 14. Time series and least squares trends in gains computed between various corrections of combined VIRS V5a and V6 and (a) Terra and (b) Aqua MODIS channel-1 radiances. V5a + V6' indicates combination of V5a data from Fig. 4 and V6 data adjusted by the normalized V6 DCC trend. V5a' denotes V5a gains adjusted to V6 responsivity. V6' / 1.0117 denotes those adjusted values that are corrected for the drop in Terra MODIS gain after day 1418.

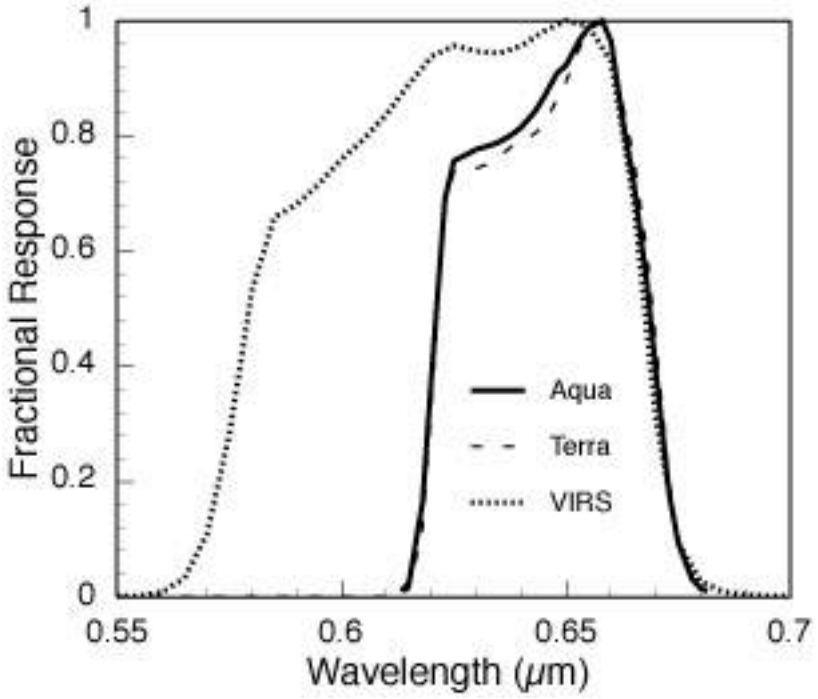

Fig. 1. Channel-1 spectral response functions.

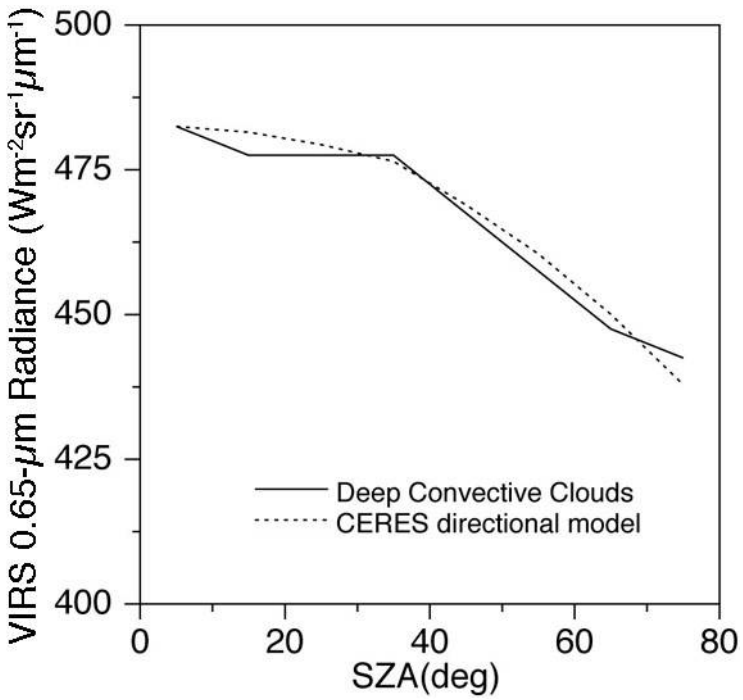

Fig. 2. Mean anisotropically adjusted radiances as a function of SZA for deep convective clouds observed from VIRS during 1998 and for the normalized CERES SZA-dependent model for ice clouds with optical depths > 50 as calibrated using the VIRS average radiance at SZA = 0°.

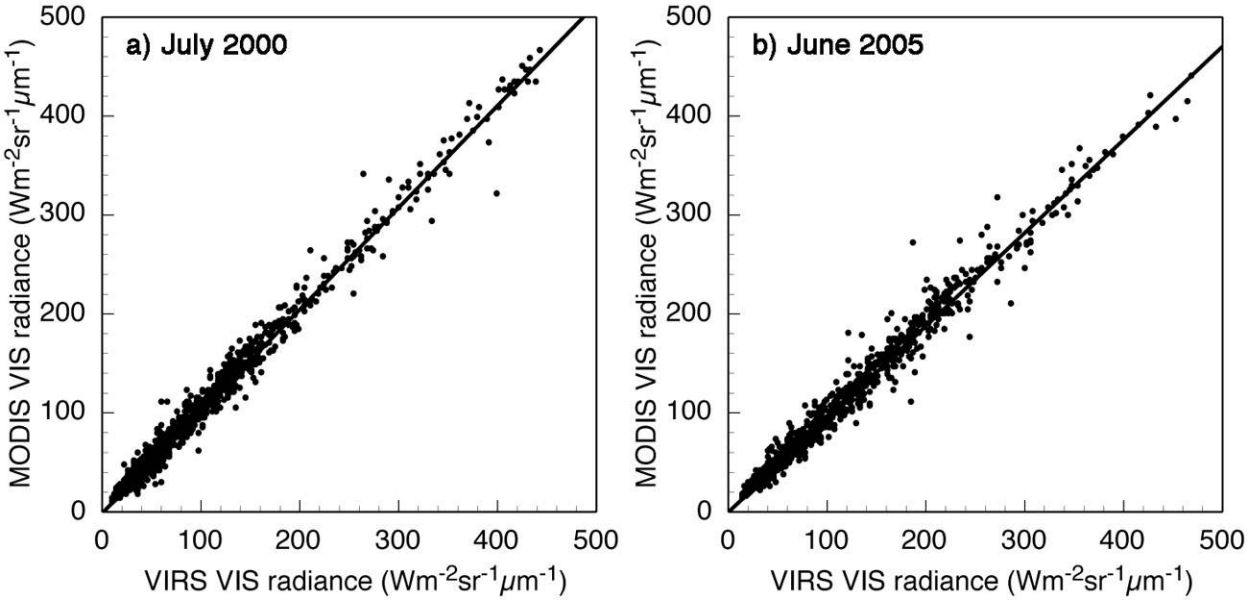

Fig. 3. Scatterplots and regression fits between VIRS and Terra MODIS VIS channels, (a) VIRS V5a, (b) VIRS V6.

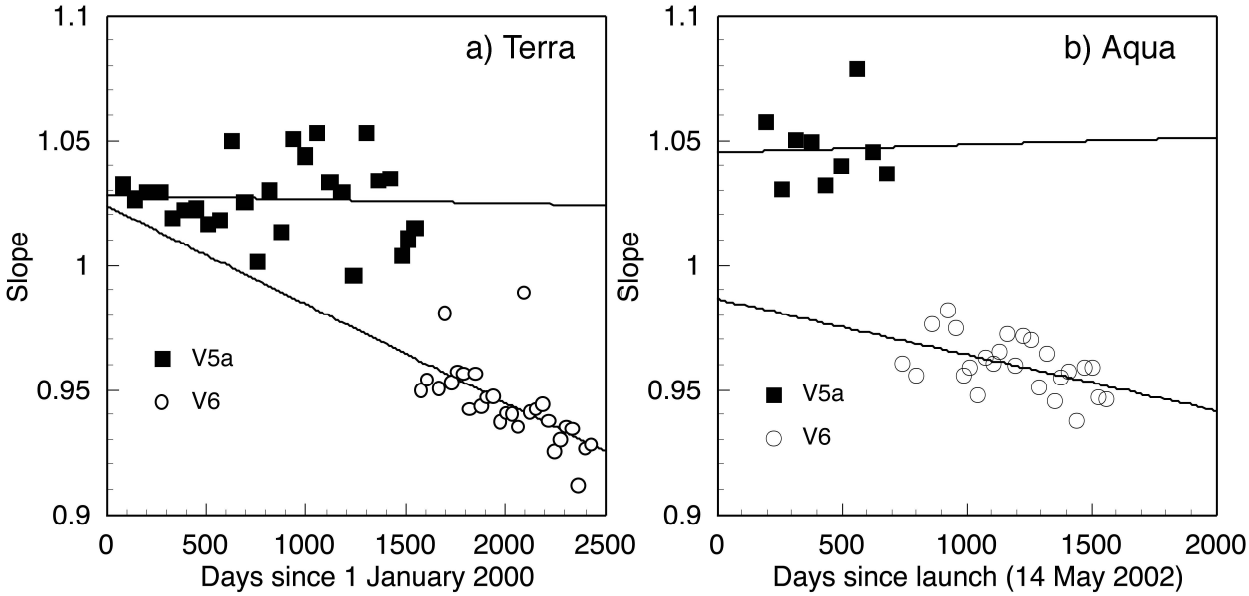

Fig. 4. Time series and least squares trends in gains computed between VIRS Versions V5a and V6 and (a) Terra and (b) Aqua MODIS channel-1 radiances.

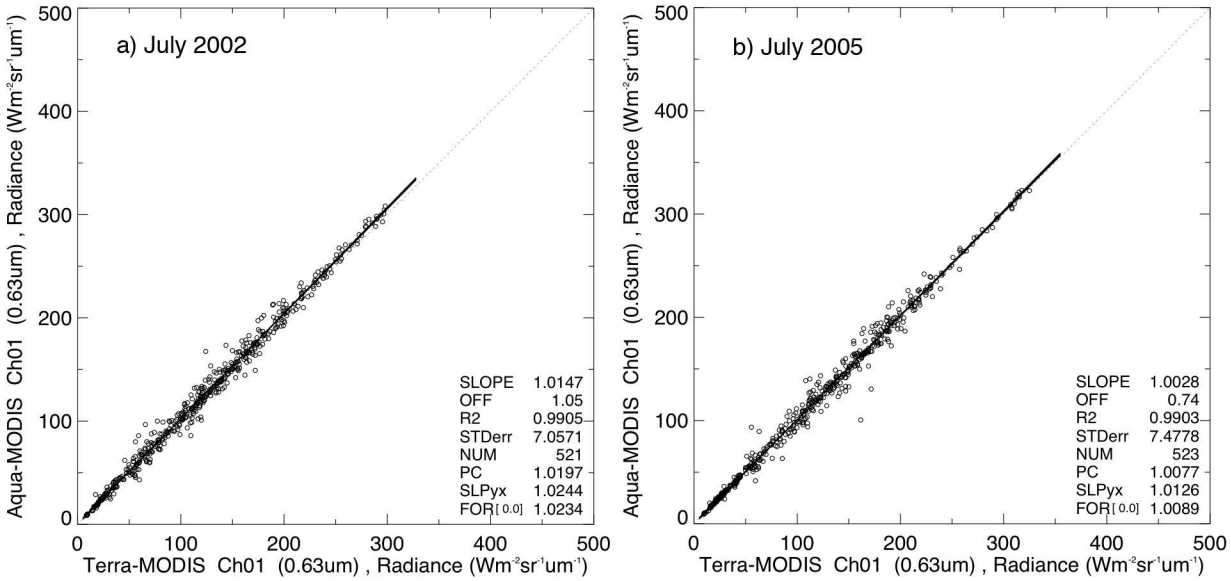

Fig. 5. Scatterplots and regression fits between Terra and Aqua MODIS VIS channels. SLOPE denotes slope for x-y fit, OFF is the x-y fit offset, and STDerr is the standard error of the fit in $Wm^{-2}\ sr^{-1}\ \mu m^{-1}$*. Only one fit is shown since the differences between the fits are negligible.*

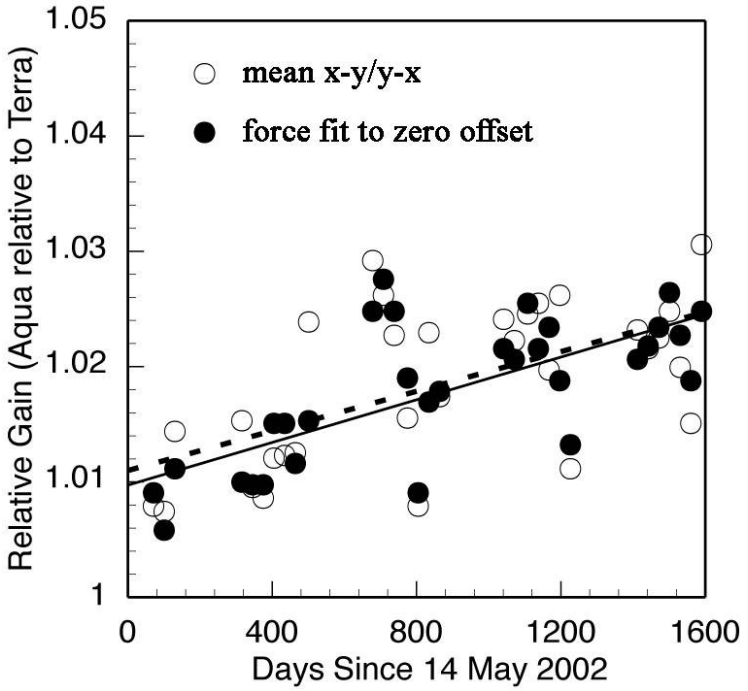

Fig. 6. Time series and least squares trends in gains computed for Aqua relative to Terra MODIS channel-1 radiances.

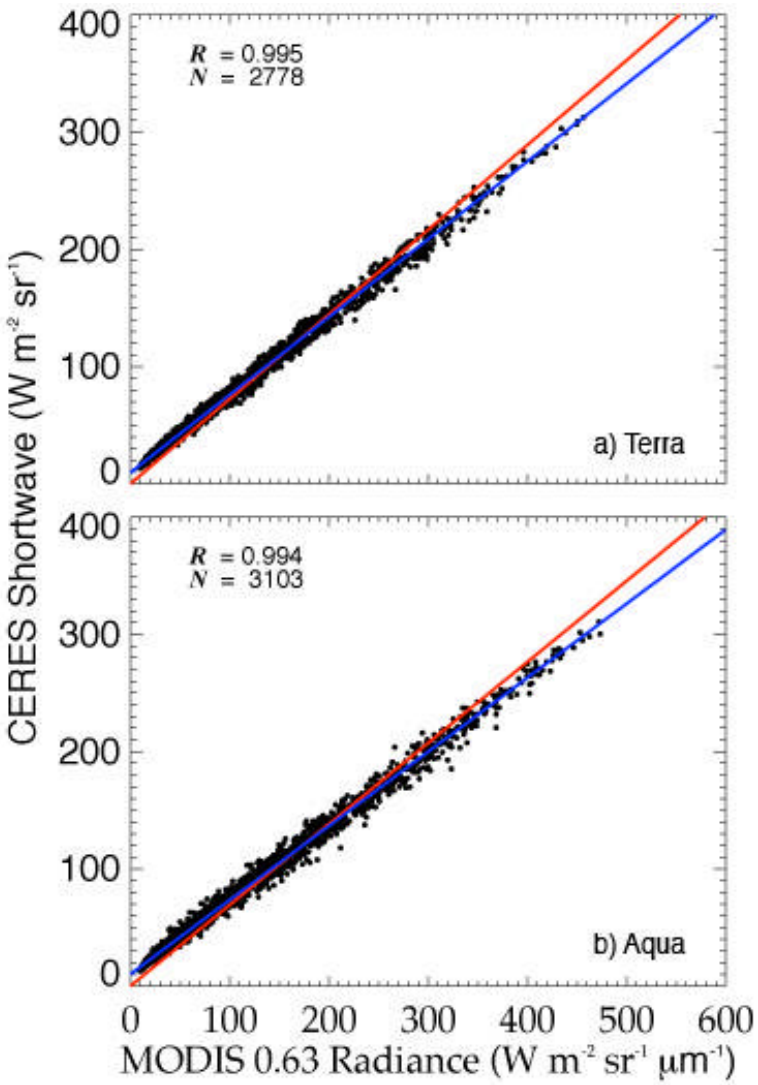

Fig. 7. Scatterplots and linear regression fits of matched CERES broadband SW and MODIS VIS radiances over ocean for 0° < SZA < 45°, 15 March 2005. Blue line is standard x-y fit. Red line is forced through the origin.

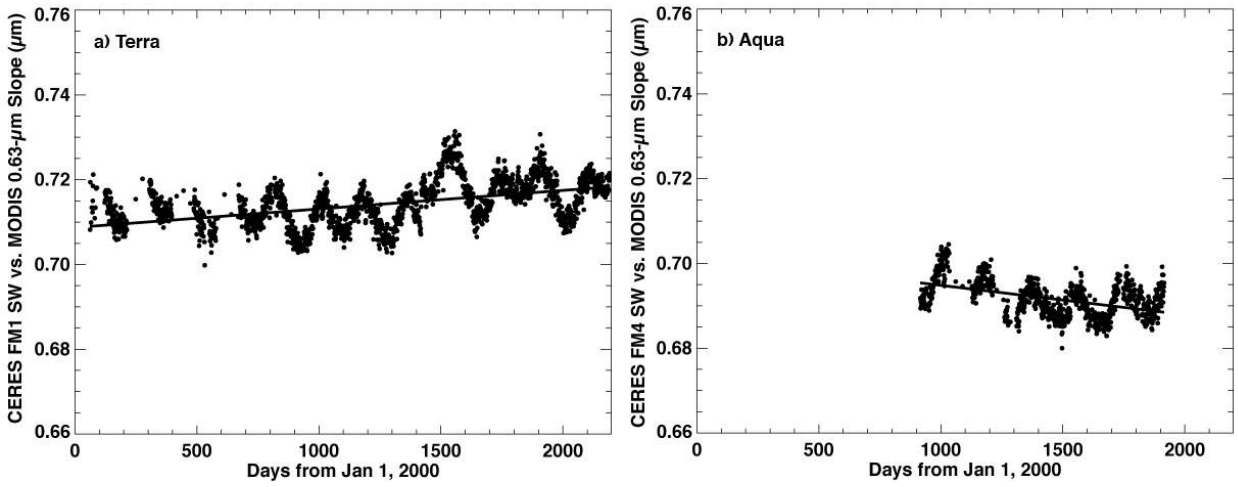

Fig. 8. Time series of daily regression slopes between CERES SW and MODIS VIS radiances over ocean for SZA between 0 and 45°.

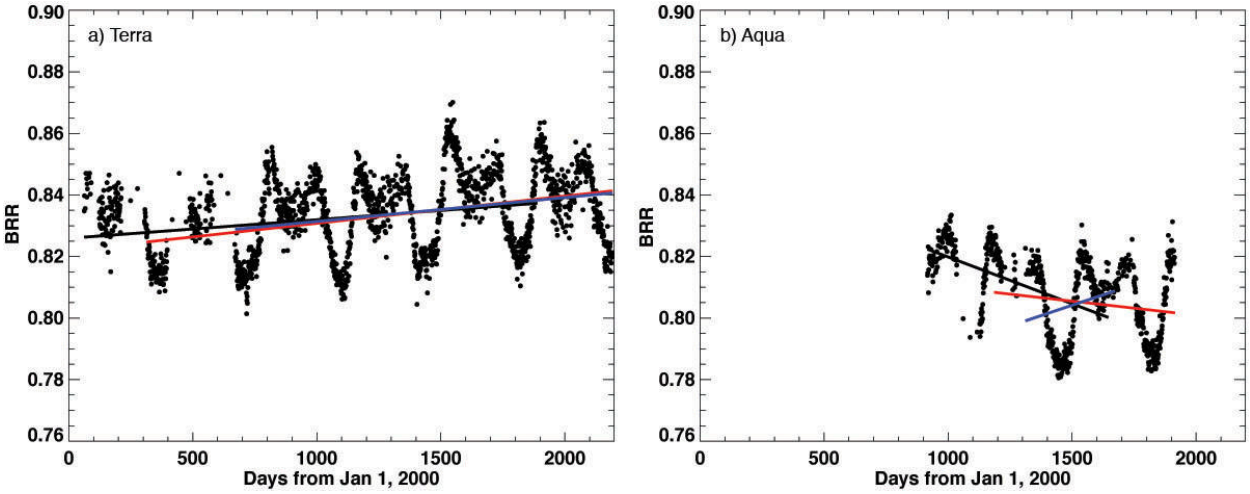

Fig. 9. Time series of daily mean bright scene bidirectional reflectance ratios of CERES SW to MODIS VIS radiances over all surfaces for SZA < 78°.

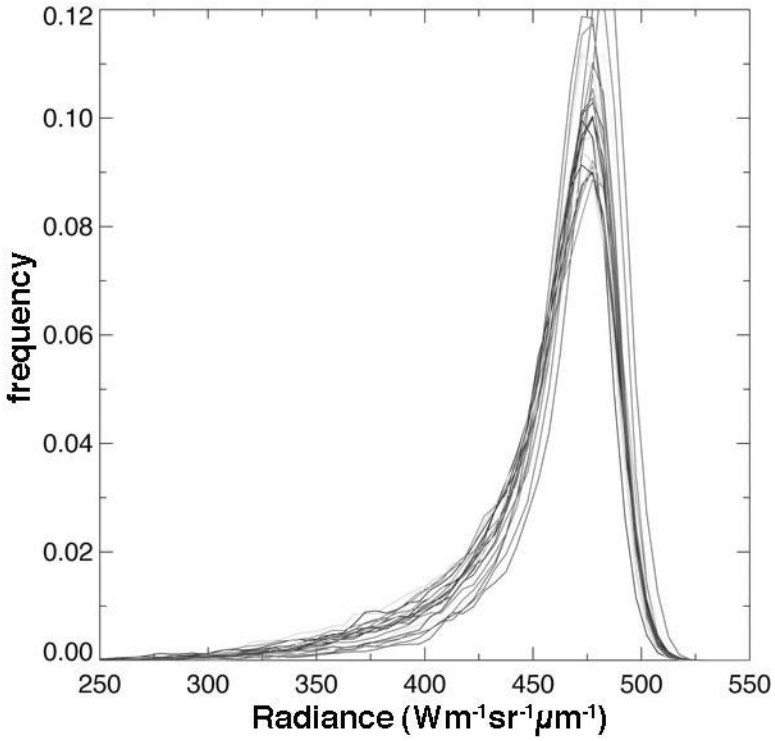

Fig. 10. Monthly probability distributions for normalized VIRS VIS radiances observed over deep convective clouds (see text) between January 1998 and April 2003.

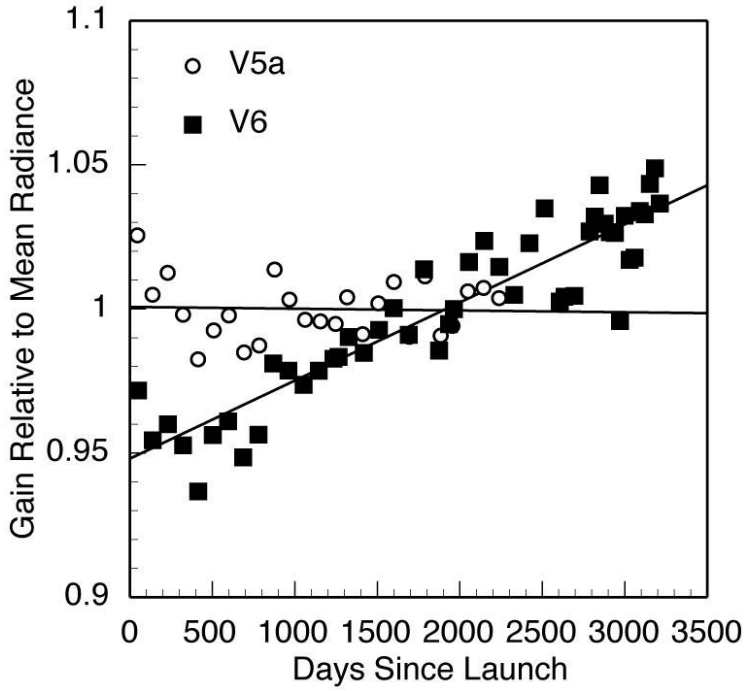

Fig. 11. Normalized trend in VIRS DCC VIS radiances relative to mean radiance of entire time series.

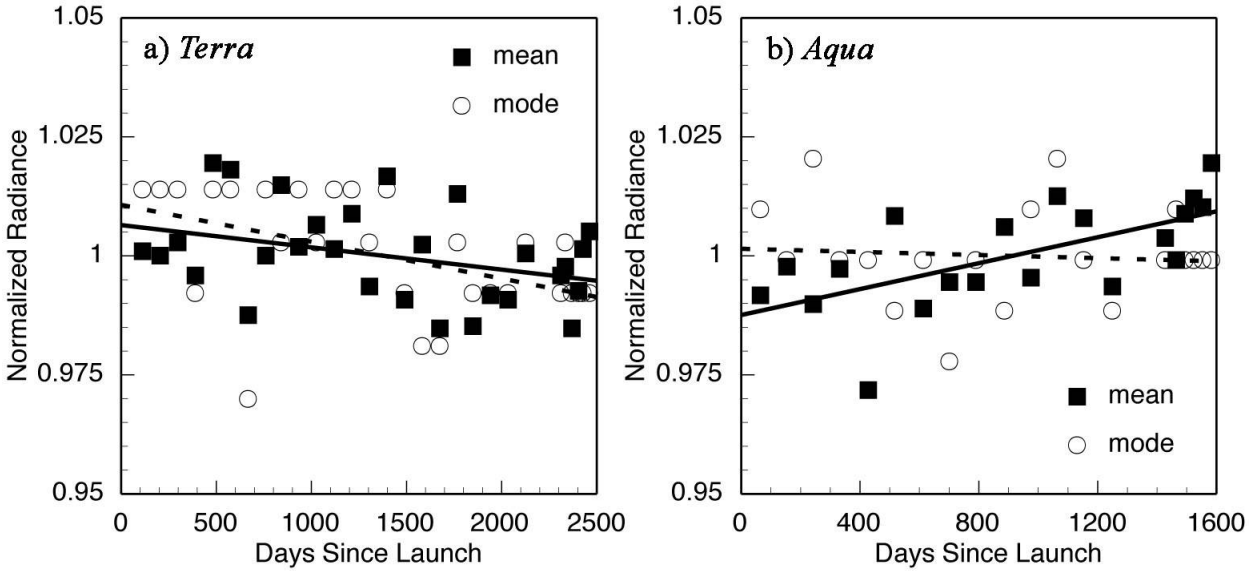

Fig. 12. Same as Fig. 11, except for (a) Terra and (b) Aqua.

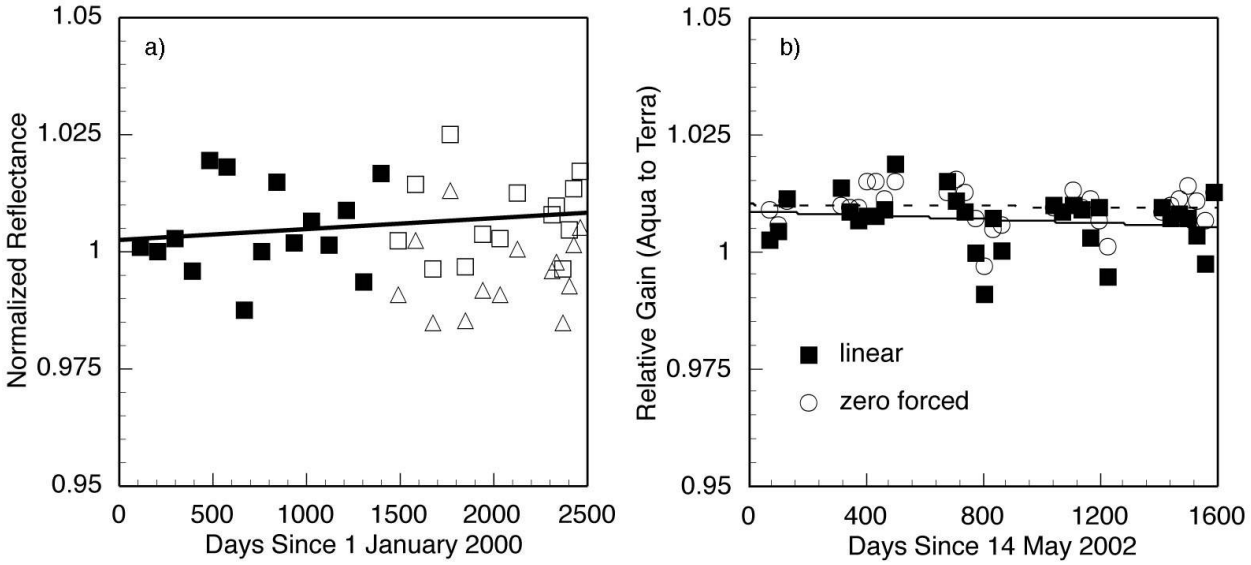

Fig. 13. (a) Monthly mean Terra MODIS VIS DCC radiances before (solid squares) and after (open triangles) day 1410 normalized to the average for entire period of record. Open squares are normalized DCC radiances taken after day 1410 that were adjusted by 1.17%, the offset found in the Terra calibration record. Line corresponds to linear regression using data corresponding to all squares. Compare to trend line in Fig. 12a. (b) Same as Fig. 6, except mean values only divided by 1.0117 after day 547. Compare solid line to dashed line in Fig. 6.

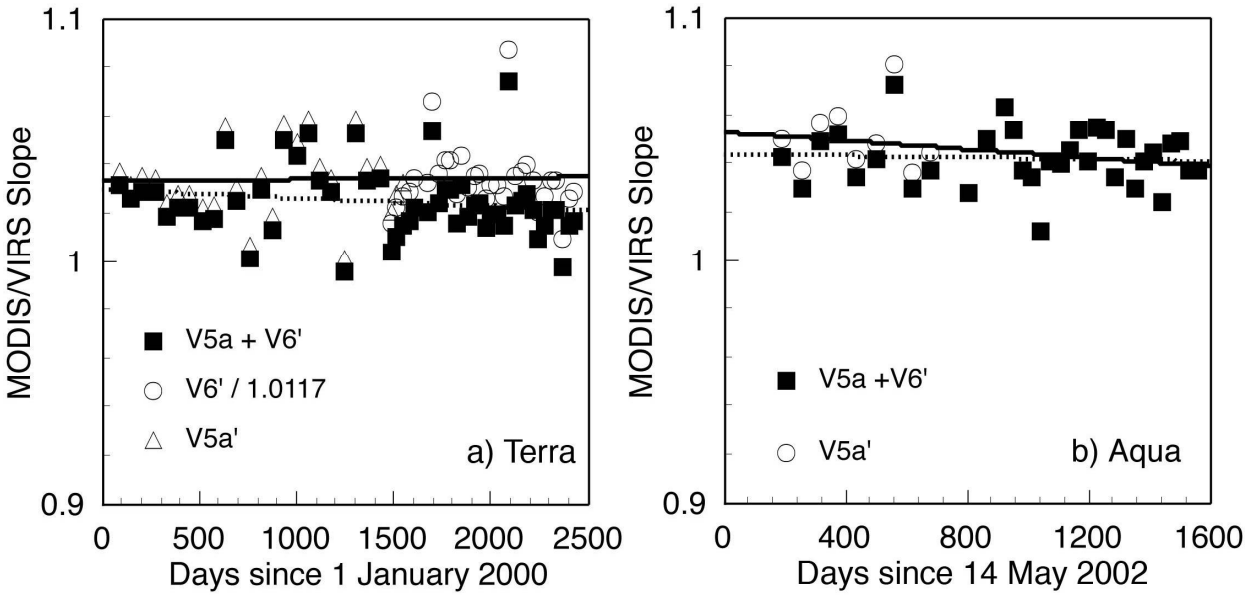

Fig. 14. Time series and least squares trends in gains computed between various corrections of combined VIRS V5a and V6 and (a) Terra and (b) Aqua MODIS channel-1 radiances. V5a + V6' indicates combination of V5a data from Fig. 4 and V6 data adjusted by the normalized V6 DCC trend. V5a' denotes V5a gains adjusted to V6 responsivity. V6' / 1.0117 denotes those adjusted values that are corrected for the drop in Terra MODIS gain after day 1418.

Table Captions

Table 1. Linear regression coefficients for raw trends in cross-satellite relative gains.

Table 2. Trends in bidirectional reflectance ratios of CERES shortwave reflectance to MODIS visible-channel reflectance referenced to 1 January 2000.

Table 3. Trends in mean normalized radiances determined from deep convective cloud analysis

Table 4. Linear regression coefficients for corrected trends in cross-satellite relative gains.

Table 1. Linear regression coefficients for raw trends in cross-satellite relative gains.

Target Satellite or Instrument	Reference Satellite or Instrument	Reference date	C_0, gain at reference date	C_1, trend since reference date		R^2
				(day^{-1})	(% y^{-1})	
VIRS V5a	*Terra*	1 Jan. 2000	1.0283	-1.615×10^{-6}	-0.06	0.002
VIRS V6	*Terra*	1 Jan. 2000	1.0242	-3.949×10^{-5}	-1.41	0.403
VIRS V5a	*Aqua*	14 May 2002	1.0455	3.047×10^{-6}	0.11	0.001
VIRS V6	*Aqua*	14 May 2002	0.9868	-2.236×10^{-5}	-0.83	0.239
Terra	*Aqua* (forced)	14 May 2002	1.0010	9.253×10^{-6}	0.34	0.506
Terra	*CERES*	1 Jan. 2000	0.7087 µm	4.378×10^{-6} µm	0.23	0.220
Aqua	*CERES*	1 Jan. 2000	0.7006 µm	-5.913×10^{-6} µm	-0.31	0.122

Table 2. Trends in bright scene bidirectional reflectance ratios of CERES shortwave reflectance to MODIS visible-channel reflectance referenced to 1 January 2000.

Target Satellite or Instrument	Time interval	C_0, gain at reference date	C_1, trend since reference date		R^2
			(day^{-1})	(% y^{-1})	
Terra	Mar. 2000 – Dec. 2005	0.8258	6.372×10^{-6}	0.28	0.085
Aqua	July 2002 –Mar. 2005	0.8665	-1.866×10^{-5}	-0.76	0.176
Terra	Mar. 2000 – Feb. 2005	0.8259	6.023×10^{-6}	0.27	0.057
Terra	Jan. 2001 –Dec. 2005	0.8219	8.846×10^{-6}	0.39	0.126
Terra	Jan. 2002 – Dec. 2005	0.8236	7.779×10^{-6}	0.34	0.071
Aqua	July 2002 -July 2004	0.8503	-3.041×10^{-5}	-1.31	0.240
Aqua	Mar. 2003 –Mar. 2005	0.8195	-9.304×10^{-6}	-0.41	0.022
Aqua	Nov. 2003 –Nov. 2004	0.7624	2.596×10^{-5}	1.24	0.058

Table 3. Trends in mean normalized radiances determined from deep convective cloud analysis.

Satellite	Reference date	Relative gain at reference date	Trend since reference date		R^2
			(day^{-1})	($\% y^{-1}$)	
VIRS V5a, mean	27 Nov. 1997	1.0001	-6.156×10^{-7}	-0.02	0.002
VIRS V5a, mode	27 Nov. 1997	1.0001	-7.516×10^{-7}	-0.03	0.008
VIRS V6, mean	27 Nov. 1997	0.9481	2.709×10^{-5}	1.04	0.845
VIRS V6, mode	27 Nov. 1997	0.9440	2.924×10^{-5}	1.13	0.925
Terra, mean	1 Jan. 2000	1.0065	-4.677×10^{-6}	-0.17	0.126
Terra, mode	1 Jan. 2000	1.0107	-7.735×10^{-6}	-0.28	0.229
Aqua, mean	14 May 2002	0.9876	1.361×10^{-5}	0.50	0.404
Aqua, mode	14 May 2002	1.0015	-1.636×10^{-6}	-0.06	0.006

Table 4. Linear regression coefficients for corrected trends in cross-satellite relative gains.

Target Satellite or Instrument	Reference Satellite or Instrument	Reference date	C_0, gain at reference date	C_1, trend since reference date	
				(day^{-1})	(% y^{-1})
VIRS V5a + V6'	*Terra*	1 Jan. 2000	1.0301	-3.381×10^{-6}	-0.12
VIRS V5a' + V6'	*Terra*	1 Jan. 2000	1.0356	-4.658×10^{-7}	-0.02
VIRS V5a + V6'	*Aqua*	14 May 2002	1.0444	-1.751×10^{-6}	-0.06
VIRS V5a' + V6'	*Aqua*	14 May 2002	1.0535	-8.827×10^{-6}	-0.31
Terra	*Aqua*	14 May 2002	1.0088	-2.103×10^{-6}	-0.08
Terra	*Aqua (forced)*	14 May 2002	1.0102	-5.080×10^{-7}	-0.02
Terra	*CERES*	1 Jan. 2000	0.7126 μm	-1.555×10^{-6} μm	-0.08